Composites: Part A 174 (2023) 107709

Contents lists available at ScienceDirect

Composites Part A

journal homepage: www.elsevier.com/locate/compositesa

3D printing asymmetric magnetic actuators with multi deformation modes

Yinduan Gao [a], Huaxia Deng [a,*], Haoming Pang [a], Bing Liu [a], Zhenbang Xu [b], Bochao Wang [a], Xinglong Gong [a,*]

[a] CAS Key Laboratory of Mechanical Behavior and Design of Materials, Department of Modern Mechanics, University of Science and Technology of China, Hefei, Anhui 230027, China

[b] CAS Key Laboratory of On-orbit Manufacturing and Integration for Space Optics System, Changchun Institute of Optics, Fine Mechanics and Physics, Chinese Academy of Sciences, Changchun 130033, China

ARTICLE INFO

Keywords:
Smart materials
Magnetic properties
Mechanical properties
Finite element analysis (FEA)
3-D Printing

ABSTRACT

Magnetic actuators have attracted widespread attention due to their advantages of fast and remote control. However, how to prepare quickly and obtain more abundant deformation modes still remains to be solved. In this paper, a composite printing powder with ultra-low modulus is developed for the preparation of asymmetric magnetic actuators. Except for the traditional bending deformation mode, the asymmetric magnetic actuators can also exhibit folding deformation mode due to the existence of gap structure. Based on the above methods, multi-dimensional asymmetric magnetic actuators are printed, and they all produce rich deformation shapes. The experimental results also show that the deformation amount of folding deformation is 5 times that of bending deformation. Finally, the experiments of butterfly wing bionics and trapper are prepared. It is proved that the magnetic actuator designed with this asymmetric structure has a broad application prospect in the field of soft robotics and bionics.

1. 1.Introduction

Inspired by the colorful deformation shapes of many biological limbs in nature, it is difficult to achieve through a single deformation mode [1]. The combination of multiple deformation types is the way to realize this bionic desire. The biomimetic of biological deformation in nature is often inseparable from soft actuators, which realize their own required deformation through various response stimuli. Common types of stimulation include light [2], heat [3], concentration [4], humidity [5], electricity [6], magnetism [7], etc. Most of the deformation generated by these stimuli is bending, which is difficult to meet the demand for multi-mode bionics. In order to obtain a variety of deformation modes, it is difficult to achieve only by changing the internal composition of materials. Therefore, it is necessary to realize other types of deformation modes through structural design [8,9].

Soft actuators that rely on magnetic stimulation have gained increasing attention due to their advantages such as fast and remote control [10]. For soft actuators, a lower modulus leads to better deformation performance [11]. The modulus of magnetorheological fluid fillers and magnetorheological plastic bodies is several orders of magnitude lower than that of magnetorheological elastomers (MREs) [12,13]. However, their initial geometry is difficult to maintain and their recovery performance is not good. In contrast, MREs are widely used in soft actuators due to their stable initial geometry and excellent cyclic loading performance [14–16]. During the first loading, the Mullins effect may occur, but the deformed shape under subsequent loading is always the same [17]. Therefore, low modulus MREs can not only enjoy the advantage of elastic recovery, but also produce ideal deformation in magnetic field, which has been continuously explored by researchers.

Due to its high residual magnetization, hard magnetorheological elastomers (H-MREs) can achieve more ideal deformation effects under the action of magnetic field [18]. As a result, H-MREs are widely used in soft actuators and have promising applications in flexible electronics [19], bionics [20], precision machinery [21], medical treatment [22], soft robotics [23] and other fields. Many studies have used H-MREs to prepare magnetic soft robots for blood vessel cleaning [24], targeted drug delivery [25], intelligent grasping [26], and bionic flowers [27]. In these H-MREs, the mode of operation is mainly bending. Under opposite magnetic fields, they bend in opposite directions. However, movements such as the flapping of an animal's wings in the air or the swimming of a frog's legs in the water involve not only bending but also folding

* Corresponding authors.
E-mail addresses: hxdeng@ustc.edu.cn (H. Deng), gongxl@ustc.edu.cn (X. Gong).

https://doi.org/10.1016/j.compositesa.2023.107709
Received 24 May 2023; Received in revised form 21 June 2023; Accepted 27 July 2023
Available online 28 July 2023

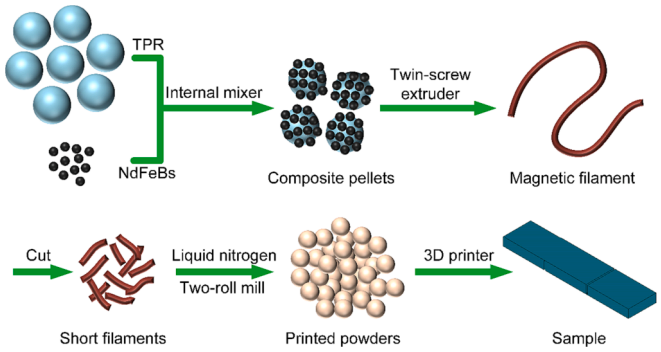

Fig. 1. Manufacturing process of H-MREs.

deformation [28]. The control source of H-MREs is mainly electromagnetic field control, and the switching of electromagnetic field can be easily achieved simply by reversing of the current. When an asymmetric structure is introduced into H-MREs, the bending and folding can be freely switched when the magnetic field is diverted, thereby better controlling the deformation of the soft actuator.

The asymmetric deformation of the structure can be achieved by the method of casting and then splicing. However, this method is cumbersome and the preparation process is difficult. Using 3D printing method to direct molding can make up for this defect [29–32]. Due to the high modulus of commercial 3D printed thermoplastic wire, the magneto-rheological elastomer prepared by doping magnetic particles also has the property of high modulus [33]. Therefore, the deformation range of H-MREs prepared with the aforementioned materials in a magnetic field is limited. In addition, the printing method of direct ink writing has also been developed for the preparation of MREs [34,35]. However, the ink produced by this method has a very low modulus, and it is difficult to form effective foundation support in complex structures with large curvature. For this reason, low modulus printing materials are prepared into wire, which can effectively print out low modulus actuators. However, materials with lower modulus, after being prepared into printing wire, experience buckling of the wire in commercial printers, making it difficult to print successfully. By preparing this low modulus wire into a powder material and using twin screw extrusion [36,37], the structural printing of ultra-low modulus H-MREs can be achieved, ensuring that the printing structure has the characteristics of low modulus and large deformation.

In order to achieve the above goals, this paper prints an ultra-low modulus H-MREs using a self-assembled powder 3D printer. The gap structure is introduced into the design of soft actuator, to form an asymmetric structure, which can realize the conversion between bending and folding deformation modes under magnetic field from different directions. The feasibility of this method is verified by mechanical three-point bending experiment and magnetic actuate experiment. It is also found that under the same loading, the deformation of folding is much larger than that of bending. Then, a variety of two-dimensional and three-dimensional soft actuators are prepared, and several types of deformation shapes are obtained. The multi-physical field simulation software COMSOL was used to simulate the deformation of these structures under magnetic field. The simulation results are in good agreement with the experimental results, showing the feasibility of this method. Finally, the simulation demonstration of butterfly wing bionics and trapper is carried out, showing the broad application prospect of this method. This method of multi-mode deformation is expected to broaden the application of MREs soft actuators in the fields of soft robotics and biomimetic.

2. Experiment section

2.1. Materials

The elastomer base material used in this study is thermoplastic rubber (TPR) with a Shore hardness of 30A, provided by the Hanwha TOTAL Petrochemical Co., Ltd. Its average particle size is about 2 mm. Magnetic particles used in this study are neodymium iron boron particles (NdFeBs) with an average size of 5 μm, purchased from BASF in Germany.

2.2. Fabrication

First, in order to remove moisture from the prepared material, the purchased TPR and NdFeBs were dried in a 50℃ oven for 24 h. Then, the two materials with a weight ratio of 1:1 are mixed by an internal mixer under the state of heating (Fig. 1) [37]. At 120℃, the surface of TPR is softened and has strong adhesion ability. NdFeBs can be successfully coated on TPR to prepare for the subsequent full mixing of the two materials. The composite particles were prepared into magnetic filament by twin-screw extruder at 150℃. A shearing tool is used to cut the magnetic filament into short filaments with an average length of 5 cm. By soaking short filaments in liquid nitrogen, the physical properties of this material are changed to a glassy state that is prone to brittle fracture. Then, the glassy filaments are quickly passed through a two-roll mill to brittle fracture. The fracture products are treated with liquid nitrogen and the gap of the two-roll mill is reduced so that further brittle failure is carried out. The short filaments can be prepared into small particle size by several steps above. Subsequently, the printed powders with particle size less than 0.6 mm was obtained by filtration through a 30-mesh screen. The printed powders were dried in a 50℃ oven for 24 h to evaporate the liquid nitrogen and water on their surface. Finally, the printed powders can be made into samples of various shapes by a 3D printer (Figure S1). The printing parameters of the printer are set as follows: the printing temperature is 200 °C, the printing rate is 3 mm/s, the nozzle diameter is 0.8 mm, the layer height is 0.2 mm, and the filling rate is 100%. The temperature of the bottom plate is room temperature, and the printing sample is fixed on the bottom plate with double-sided adhesive. The printed samples were magnetized for 10 min at a magnetic flux density of 1.5 T. During the magnetization process, the sample is first fixed to the expected deformation shape with external force, and then magnetized. After magnetization, the external force is removed to obtain different magnetization directions.

2.3. Characterization and instruments

The samples were printed using a self-assembled powder 3D printer. The micromorphology of the printed powder and samples were characterized by optical microscope (OM, VHX-200). The magnetic properties of TPR, NdFeBs and H-MREs were measured by hysteresis loop meter (HyMDC Metis, Leuven, Belgium). Uniaxial tensile tests of printed materials and three-point bending tests of asymmetric structures were performed using a dynamic mechanical analyzer (DMA, ElectroForce 3200, TA instruments, Minnesota 55344 USA). All deformation experiments under magnetic field were performed by electromagnet (XDA-200/80/60, Yueqing Xingda Electric Co., Ltd., China). A computer-controlled program power supply (ITECH IT6724) generates the current required for the electromagnet. The flux density was measured using a Tesla meter (HT20, Shanghai Hengtong Magnetic Technology Co. Ltd, China).

2.4. Numerical methods

COMSOL Multiphysics 6.0 was used to analyze the deformation of asymmetric structures under three-point bending loading and magnetic field actuation. Only the solid mechanics module was used in the three-

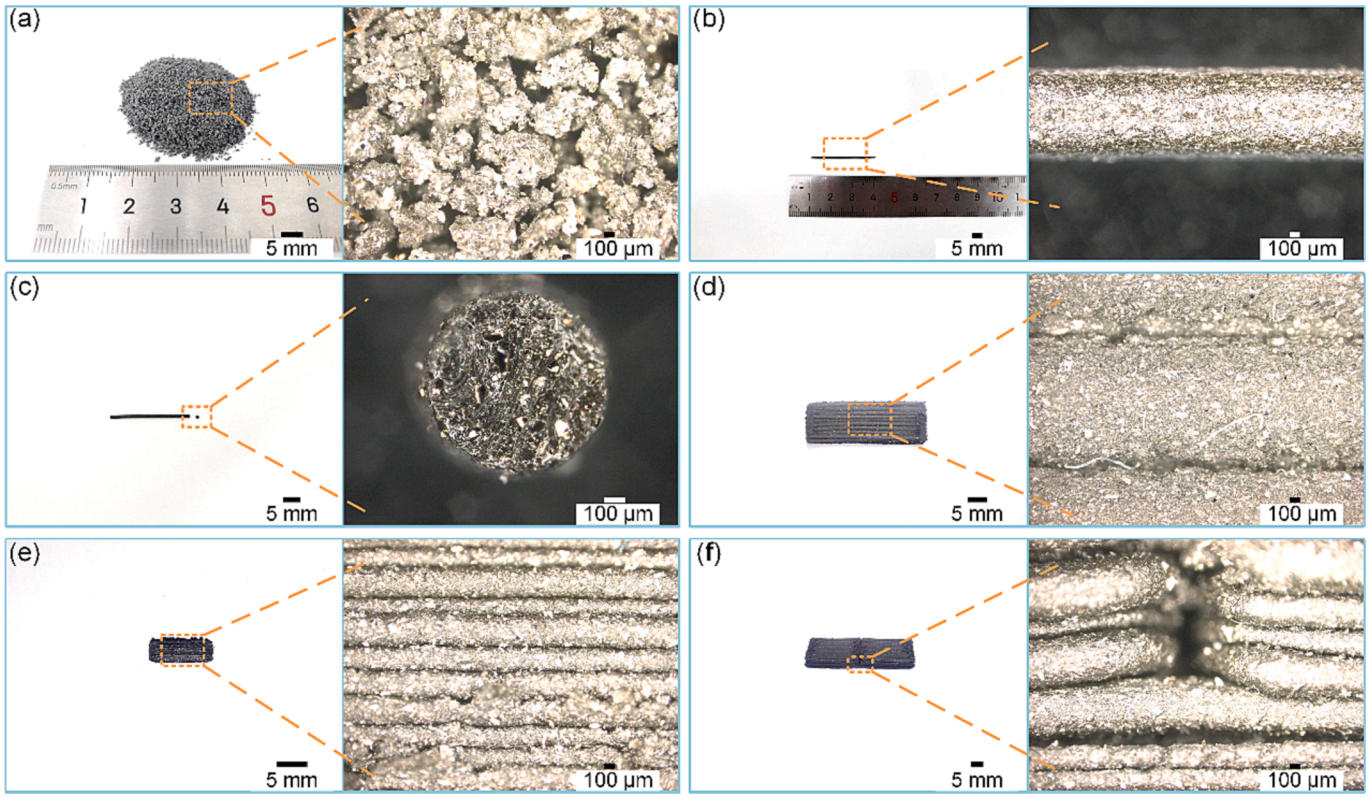

Fig. 2. The microstructure of the sample. (a) Printing powder. (b) Extruded wire. (c) Wire section. (d) Upper surface of the sample. (e) Side of sample. (f) Asymmetric structure.

point bending deformation, and the load was applied by specifying the displacement of the loading device. The magnetic field module and solid mechanics module were used to solve the magnetic field induced deformation. The sample model and the electromagnet model were established, and the air domain for analyzing the magnetic field distribution was also established. Firstly, magnetic field module analysis was carried out to obtain the distribution of magnetic field in the entire calculation area. The sample was set as a magnetized material, which was subjected to the force of a magnetic field. It was then loaded to the sample surface as a surface Maxwell stress tensor in the solid mechanics module. After finite element solution, the deformation results of the sample under the action of magnetic field were obtained.

3. Results and discussions

3.1. Microstructure of powder materials and printed samples

The microstructure of the printed sample determines its mechanical properties. Therefore, the sample structure was observed by optical microscopy (Fig. 2). Powder printing materials (Fig. 2a) are prepared by grinding and vary slightly in size and shape. However, after it is screened by the screen, large particles are removed, and the size of the remaining particles is kept at about 0.6 mm, which ensures that these materials pass smoothly in the printer. The wire printed by the printer is shown in Fig. 2b, demonstrating a uniform thickness across the entire section. As the diameter of the printer nozzle is 0.8 mm, the diameter of the wire is slightly higher than 0.8 mm. This is because the molten material is extruded through the nozzle, after which the material experiences no pressure action and the wire expands slightly. The cross-section diagram of the printed wire is shown in Fig. 2c. The cross-section shape is circular, and it is found that the material is uniform in the cross section, indicating that TPR and NdFeBs are fully mixed. In Fig. 2d and Fig. 2e, the upper and side surfaces of the sample are observed. The upper

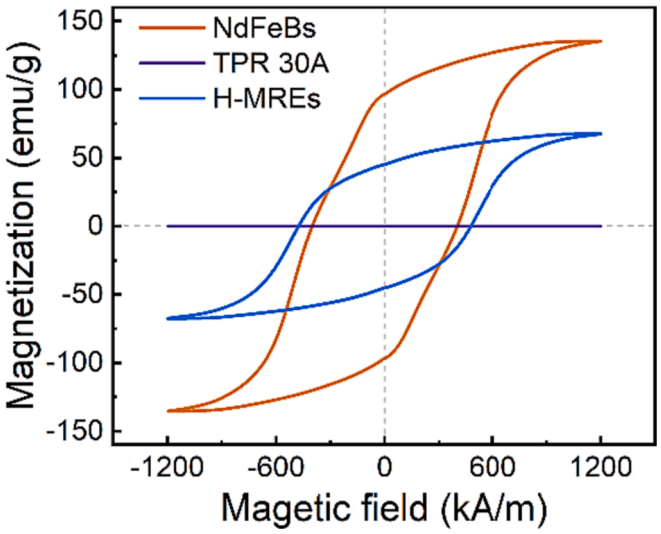

Fig. 3. Hysteresis loop of materials.

surface wire of the sample is 1.2 mm wide, wider than the material coming out of the nozzle at 0.8 mm. This is because the height is set at 0.2 mm, and the height printed out is smaller than the diameter of the printed wire (Fig. 2e). During the process of sample printing, the wire is pressed by the nozzle, resulting in the height of the wire being smaller and the width being larger. Finally, the asymmetric position of the sample was observed (Fig. 2f). When printing, the printer is disconnected at an asymmetric position, ensuring that the sample forms a gap at this position, resulting in asymmetric deformation.

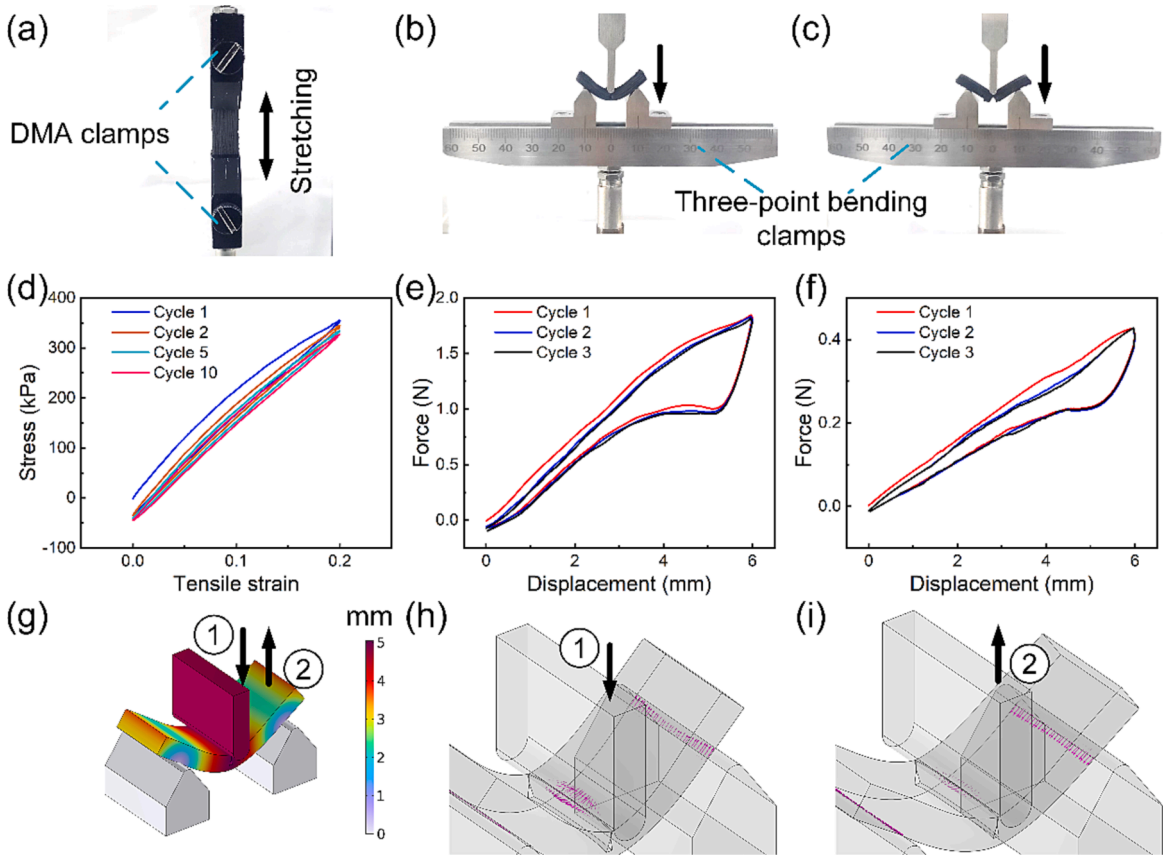

Fig. 4. Mechanical properties of asymmetric structures. (a) Uniaxial tensile test facility for printing materials. (b-c) Three point bending loading device with asymmetric structure in different directions. (d) Stress–strain curve of uniaxial tensile. (e-f) Force-displacement curve under three point bending load. (g) Simulation analysis diagram of three point bending experiment. (h-i) Friction distribution during loading and unloading.

3.2. Magnetic properties of materials

In order to obtain the magnetic properties of the materials used, hysteresis loops of the materials were tested by hysteresis loop meter (Fig. 3). In this figure, NdFeBs, TPR and H-MREs were tested respectively, and M-H curves of these materials were obtained. In the experiment, 1200 kA/m was selected as the maximum magnetic field intensity. Near the maximum magnetic field intensity, the magnetization of the material has stabilized, which meets the test requirements. The experiment results show that NdFeBs and H-MREs are hard magnetic materials with saturated hysteresis loops. Meanwhile, the magnetization of the TPR is always 0, indicating that the material will not interact with the magnetic materials in magnetic field. According to the experimental data, the saturation magnetization of NdFeBs was 135.2 emu/g, the residual magnetization was 96.7 emu/g, and the coercivity was 400.2 kA/m. The corresponding parameters of H-MREs are 67.5 emu/g, 47.6 emu/g and 475.8 kA/m, respectively. It is found that the saturation and residual magnetization of H-MREs are about half of that of NdFeBs. The main reason for this phenomenon is that in the preparation of H-MREs, the mass ratio of NdFeBs and TPR is 1:1. The reason for their different coercivity is that the NdFeBs particles cannot be completely fixed during testing, and a small part of the particles rotate with the loading of the magnetic field. In contrast, the relative positions of magnetic particles in H-MREs remain unchanged. Therefore, the coercivity of H-MREs is greater than that of NdFeBs.

3.3. Mechanical properties of asymmetric structures

In order to obtain the mechanical properties of the asymmetric structures, the printed samples were tested by DMA uniaxial tensile test and three-point bending test (Fig. 4). First, the uniaxial stretching experiment of cuboid sample (Fig. 4a) was tested to obtain the elastic modulus of the printing material. The size of the cuboid sample is set as $30 \times 10 \times 2$ mm, in which the length of the test section is 20 mm. During the test, the tensile strain rate was set at 0.01 s^{-1} and the maximum tensile strain was 0.2. Ten cycles of stretching tests were performed, and the stress–strain curves were shown in Fig. 4d. The material showed Mullins effect in the first stretch, and the rest of the stretch showed a linear relationship. The calculated elastic modulus of the material is 1.8 MPa. The enclosed area of the stress–strain curve indicates the energy loss of the material. After many times of loading, loading and unloading curves almost coincide, which indicates that the material has litter energy dissipation and good elastic properties. The structure of this material is robust when it is used for magnetic actuation, and there will be no deviation due to multiple uses. In addition, force–displacement curves of asymmetric structures loaded in different directions were tested by a three-point bending loading device (Fig. 4b-c). The geometry of the test structure is $30 \times 10 \times 3$ mm. The gap is arranged in the middle of the structure. The gap width is 0.5 mm and the depth is 2.6 mm. The distance between the two fulcrum of the three-point bending fixture is 20 mm, and the maximum pressing depth during loading is 6 mm. Loading in different directions causes the structure to show two deformation modes: bending and folding. The force–displacement curves of bending deformation and folding deformation are shown in Fig. 4e and Fig. 4f, respectively. At the maximum loading displacement, the maximum loading force required for bending deformation mode is 1.81 N, while that for folding deformation mode is 0.42 N. As can be seen from the figure, the introduction of gap structure makes the structure show asymmetry. Under the same loading force, the folded deformation mode produces a larger deformation displacement. As demonstrated in

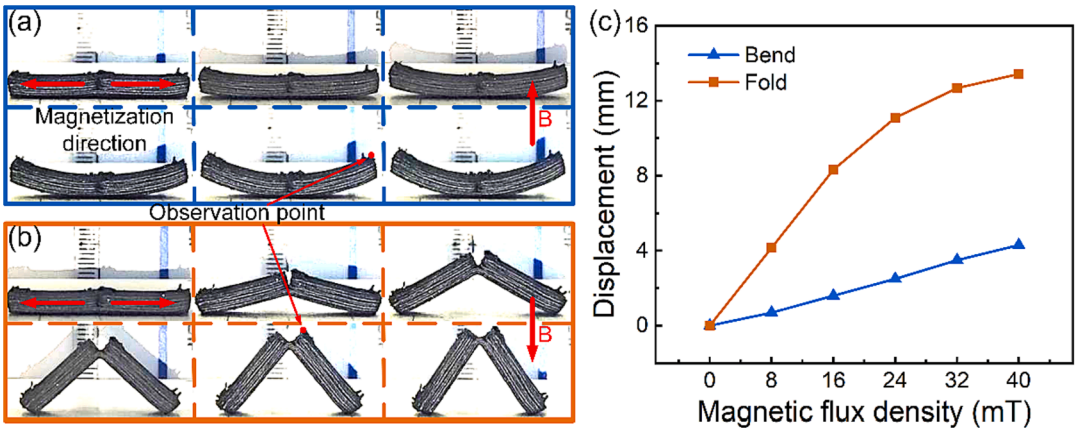

Fig. 5. Deformation of asymmetric structure under magnetic field. (a) Bending deformation mode. (b) Folding deformation mode. (c) Deformation statistics of two deformation modes.

the three-point bending loading curves, the force will suddenly decrease at the beginning of the unloading stage, and then gradually become consistent with the loading stage curve. In order to explain this phenomenon, the simulation of three-point bending loading experiment was carried out in this paper (Fig. 4g). The friction force distribution of simulation results is analyzed. Fig. 4h corresponds to the distribution of friction force during loading. It can be seen from the figure that the component of friction force in the vertical direction is upward. Fig. 4i shows the distribution of friction during unloading, with the vertical component pointing downward. The direction of friction is always opposite to the direction of relative deformation. However, from loading to unloading, the direction of friction reverses. It is because of the change in the direction of friction that the force–displacement curve in the experiment suddenly drops at the beginning of unloading.

3.4. Comparison of magnetic actuation asymmetry of structures

In order to verify that the above asymmetric structure also exhibits the characteristics of multiple deformation modes under magnetic field, deformation experiments were conducted under different flux densities

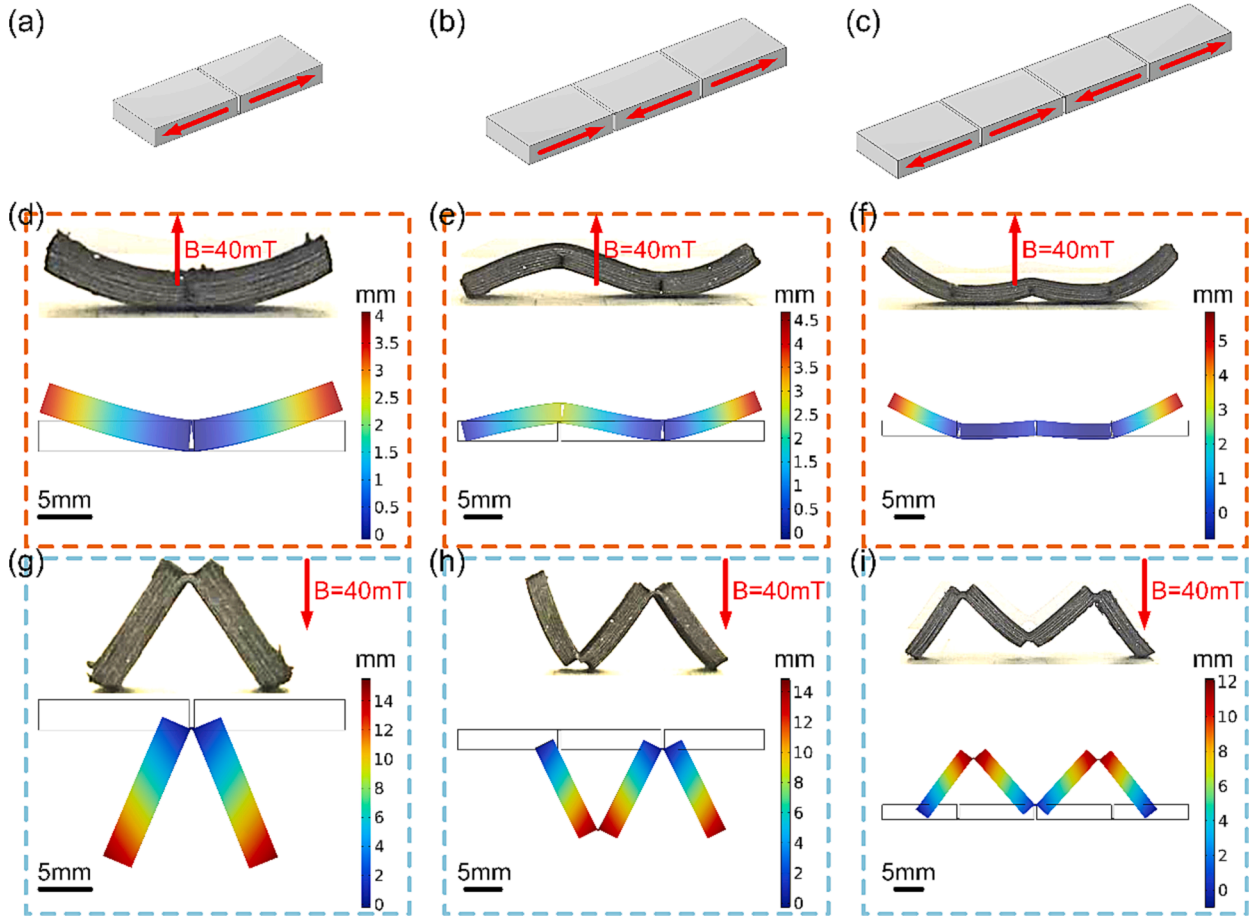

Fig. 6. One-dimensional asymmetric structure. (a-c) The structure with different segments. (d-f) Bending deformation of three structures. (g-i) Folding deformation of three structures.

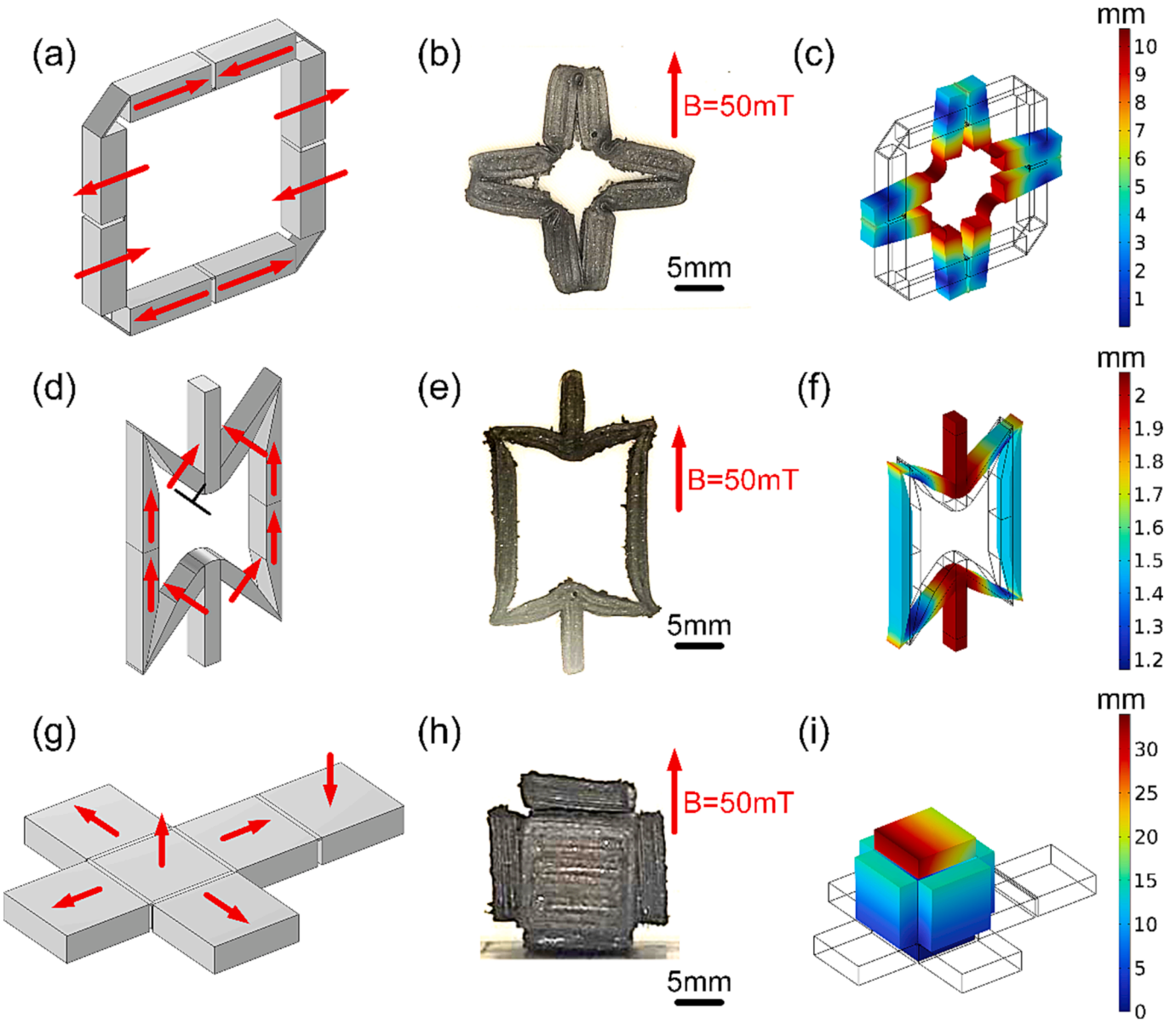

Fig. 7. Two-dimensional and three-dimensional asymmetric structures. (a-c) Star structure. (d-f) Negative Poisson's ratio structure. (g-i) Cube structure.

and magnetic field directions as shown in Fig. 5. The direction of magnetization of the structure is also demonstrated in this figure. On both sides of the gap structure, the magnetization directions are respectively in the left and right directions. When a magnetic field is applied, the magnetic field exerts magnetic force on hard magnetic materials, and the magnetization direction of materials will tend to rotate in the direction of magnetic field application. When an upward magnetic field is applied (Fig. 5a), the two sides of the structure tend to rotate upward. Due to the small width of the gap structure, the left and right sides of the structure contact quickly, resulting in bending deformation. As the magnetic field increases, so does the degree of bending. When a downward magnetic field is applied (Fig. 5b), the left and right sides of the structure rotate in opposite directions and rotate downward. Without the gap structure, the structure will still experience bending deformation, but there will not be multiple deformation modes. Due to the existence of the gap structure, the upper part of the left and right sides of the structure are separated and no longer provide flexural stiffness. Only the lower part provides flexural stiffness. Compared with the middle part, the left and right sides of the structure have greater flexural stiffness, so the deformation is mainly concentrated in the middle part, and the left and right sides only produce approximate rigid body displacement. It is for this reason that a new deformation mode, folding, has emerged. As the magnetic field increases, so does the folding deformation. In Fig. 5c, the deformation sizes of these two deformation modes under different magnetic fields are calculated. Compared to the deformation size of bending deformation, By comparison, the deformation size of folding deformation is much higher than that of bending deformation. With the increase of magnetic field increases, the deformation of folding deformation increases faster. And the folding deformation quickly approaches the limit of 15 mm, the curves thus presenting the platform segment in the image. When the loading flux density is 20 mT, the deformation of the two deformation modes is about 2.0 mm and 9.7 mm, and the difference between them is nearly five times. The introduction of this asymmetric structure significantly increases the amount of deformation caused by magnetic actuation. At the same time, it also means that the introduction of asymmetric structures will allow the magnetic actuator to operate under a smaller magnetic field. To illustrate the fatigue stability of this printing material, the deformation amount under 1000 cycles of loading and unloading is shown in Figure S2.

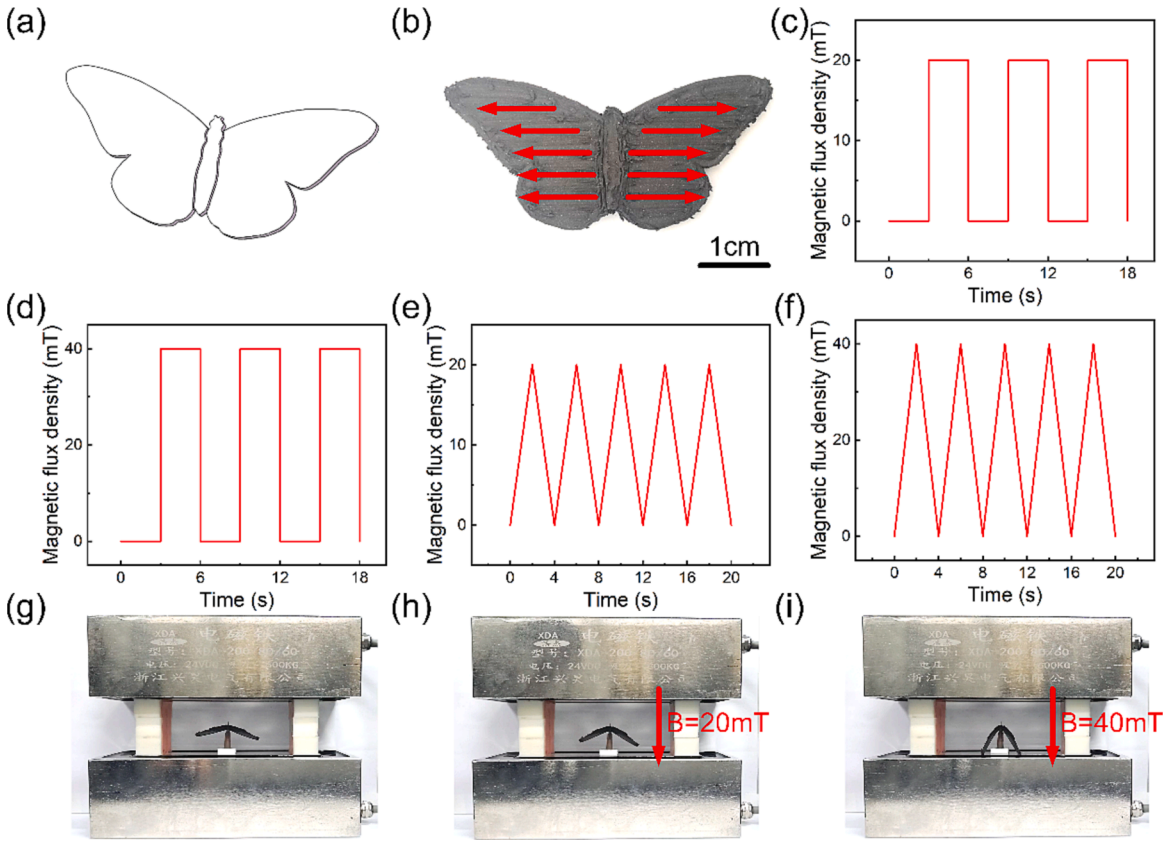

Fig. 8. Butterfly wing bionics demonstration experiment. (a) Model structure. (b) Magnetization direction of the wings. (c-f) Different types of magnetic field signals. (g-i) Deformation of wings under different magnetic fields.

3.5. One-dimensional asymmetric structure

This asymmetric structure can realize the diversity of the deformation of the magnetic actuator. A variety of one-dimensional asymmetric structures were printed by 3D printer, and the deformation shapes of different structures under magnetic field were analyzed through experimental verification and simulation calculation (Fig. 6). The finite element model is a three-dimensional model and only provides a front view for comparison with the experiment. The simulation deformation map and the experimental deformation map are in good agreement. Three one-dimensional asymmetric structures are shown in Fig. 6a-c. They introduce one, two, and three gap structures, respectively, dividing the long sample into different segments. When the structure is magnetized, the direction of magnetization of adjacent sections is different. Under the action of a vertical upward magnetic field, the structure mainly exhibits bending deformation (Fig. 6d-f). When a downward magnetic field is applied, the structure deformation is mainly folded (Fig. 6g-i). In Fig. 6d and Fig. 6f, the bending deformation of the two - and four-segment asymmetric structure is a left - and right-sided symmetrical shape. In Fig. 6e, the bending deformation of the three-segment asymmetric structure presents a central symmetric deformation. The same phenomenon can be seen in the folding deformation caused by the downward magnetic field. This is related to the parity introduced by asymmetric structures. In Fig. 6f, the upward deformation of the two ends is greater than that of the middle. This is because the two ends are free ends and their deformation is mainly determined by the force exerted by the magnetic field. While being subjected to a magnetic field force in the middle, it is also subjected to an elastic resistance force applied from the other side. This force acts in the opposite direction of deformation, so the middle deforms less than the sides. In Fig. 6i, there is also a phenomenon that the middle deformation is small, but the difference between the middle deformation and the deformation at both ends is reduced. This is because the contact between the left and right sides is much smaller than when bending, thus the elastic resistance is relatively small. It is found that the folding deformation of the three structures is always greater than the bending deformation. The above results show that the asymmetric structure plays a significant role in one-dimensional structures, and the deformation modes of the structures have been greatly enhanced.

3.6. Two-dimensional and three-dimensional asymmetric structures

Asymmetric structures can be applied not only to one-dimensional magnetic actuation structures, but also to two-dimensional and three-dimensional structures (Fig. 7). Previous experiments have demonstrated that folding deformation can lead to greater deformation amounts. Based on this large deformation principle, more abundant magnetic actuation deformation can be designed. Firstly, asymmetric structures are applied to the magnetic actuation deformation of two-dimensional star structure (Fig. 7a-c). In 3D printing, hollow square structures are printed. The square's four corners and the midpoints of its four sides are designed with asymmetrical structures. At the four sides, the asymmetrical structures are designed to the outside. Thus, the structure is divided into several segments, and the magnetization directions of different segments are shown in Fig. 7a. Under the action of a magnetic field, a star-shaped deformation occurs. Experimental and simulation results verify the effectiveness of the star structure deformation. Subsequently, a two-dimensional negative Poisson's ratio structure is designed (Fig. 7d-f). The gap structure is designed in the four corners of the structure to enable greater relative rotation between the inclined beam and the vertical beam. Under the action of a magnetic field, there is a positive deformation in the vertical direction. At the same time, the lateral deformation is also positive. The relative strain in both directions is positive, resulting in negative Poisson's ratio

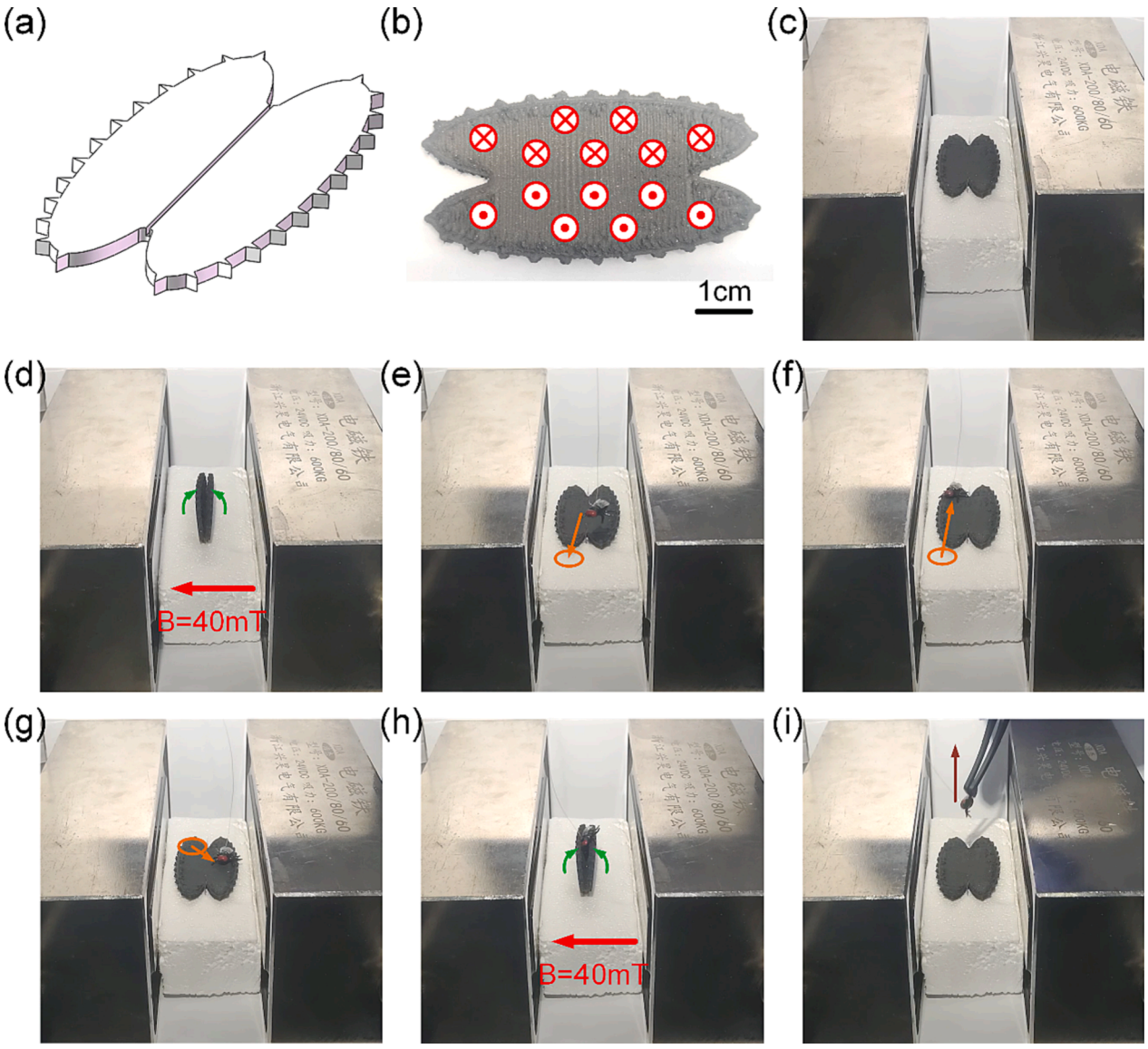

Fig. 9. Trapper demonstration experiment. (a) Model structure. (b) Magnetization direction of the trapper. (c-d) The deformed state of the trapper. (e-i) The grasping process of the trapper.

phenomenon. Finally, asymmetric structures are applied to three-dimensional deformation (Fig. 7g-i). In a printed two-dimensional plane structure, the asymmetric structure is designed at the position where it needs to be folded. Different regions of the structure are magnetized in different directions. Under the action of a magnetic field, large folding deformation occurs at the gap structure, and finally a three-dimensional cube structure is formed. The above experiments prove that asymmetric structures have a wide application space in higher dimensions.

3.7. Application experiment

Asymmetric structures have wide application space in magnetic actuation bionic deformation. The use of asymmetric structures applied to butterfly wings can produce large deformations (Fig. 8). A butterfly model is designed, as shown in Fig. 8a, and a gap structure is set at the connection position of wings and body. The wings were then magnetized, with both wings magnetized outwardly (Fig. 8b). Then, a computer-controlled program-controlled power supply is applied to the electromagnet to generate a square wave magnetic field (Fig. 8c-d) and a triangular wave magnetic field (Fig. 8e-f) that change with time. Square wave signals are used to simulate the instantaneous flapping of wings, while triangle wave signals are used to simulate the slow flapping of wings. Two amplitude tests were performed for both types of signals, respectively 20 mT and 40 mT. Under the action of these two amplitude signals, the vertical amplitude of the wings reaches 8 mm and 15 mm respectively. The shape of the butterfly without magnetic field is shown in Fig. 8g. The two wings fell slightly due to gravity. Under the action of a magnetic field with a amplitude of 20 mT, the maximum deformation of butterfly wings is shown in Fig. 8h. By further increasing the amplitude of the applied magnetic field, the maximum deformation of the wing will be larger, thus reaching the position shown in Fig. 8i. Under the multi-period action of square wave signal and triangle wave signal, butterfly wings will change repeatedly between the initial position and the maximum position. The position does not shift due to repeated action, which proves that the magnetic material has better elastic properties. When applying a square wave signal, the flapping of the wings is an instantaneous process, corresponding to the rapid flapping of the butterfly's wings. Under the action of triangular wave signals, the flapping of wings is a slow process, corresponding to the light flapping of butterfly wings (Supplementary Movie S1). In the bent wing flap, the deformation is mainly concentrated on the wing tip. However, in the

folded deformed wing flap above, the deformation is widely distributed in the whole wing position. Therefore, this folding deformation is more likely to be applied to magnetically actuation flight, resulting in greater upward lift.

In addition, inspired by the Venus flytrap, the application of asymmetric structures to magnetic actuation trapper is also investigated (Fig. 9). First, the trapper model is designed, as shown in Fig. 9a. The two sides of the trapper adopt oval design, and a gap structure is designed in the middle to produce large deformation. Then magnetize both sides of the trapper in the directions of vertical paper facing outward and vertical paper facing inward (Fig. 9b). Fig. 9c shows the deformation of the trapper in the absence of a magnetic field, with the two sides of the trapper opening horizontally. Fig. 9d shows the deformation of the trapper in the presence of a magnetic field, with the two sides of the trapper rapidly merging. Its merging speed is within 0.1 s. Fig. 9e-i shows the whole process of the trapper capturing the prey. In Fig. 9e, the prey flies and lands next to the trapper, at which time no magnetic field is applied, and the trapper is in an open state. Subsequently, the prey flew to a corner of the trapper (Fig. 9f), as this position was not the optimal grasping position, so the magnetic field was still closed. When the prey flies near the center of the trapper (Fig. 9g), a magnetic field is suddenly applied. The trapper quickly closes under the action of the magnetic field, thus successfully capturing the prey (Fig. 9h). Finally, the tool is used to clamp the prey and turn off the magnetic field. At this time, the trapper changes from the closed state to the open state (Fig. 9i). The prey is clamped by the tool and the trapper waits for the next grab (Supplementary Movie S2). Through the above experiments, it is verified that the magnetic actuation trapper can produce fast and large deformation response by using the slit structure, so as to successfully capture prey. The trapper produces a large 180° deformation through the folding deformation mode, which is difficult to achieve in the bending deformation. The simulation experiment of trapper also proves that asymmetric structures can be widely used in magnetic actuation deformation.

4. Conclusion

In summary, this work has developed an H-MREs asymmetric structure with ultra-low modulus. For this purpose, the printing powder was first prepared by NdFeBs and TPR 30A, and the asymmetric structure was prepared by a self-assembled 3D printer. Then, the uniaxial tensile test proves that the TPR 30A matrix printing material has very low modulus indeed. Through three-point bending experiment and magnetic actuation experiment, it has been proven that asymmetric structure can not only generate bending deformation mode, but also folding deformation mode. The experimental results show that under the same loading condition, the deformation amount of folding deformation mode is about 5 times that of bending deformation mode. Subsequently, this asymmetric structure is applied to multi-dimensional magnetic actuators, which can generate rich deformation shapes. The deformation of the magnetic actuators are analyzed through a combination of experimental verification and finite element simulation methods, and the results are very consistent, jointly proving the effectiveness of this asymmetric structure. Finally, the application value of this asymmetric structure is verified by applying it to butterfly wing flapping and trapper. In the application experiment of butterfly wings, the flapping of the wings changes from the original tip flapping to the entire wing flapping. Meanwhile, in the experiment of the trapper, it generated a large deformation range of 180°, which is difficult to achieve in traditional bending deformation mode. This study proves that the design of this asymmetric structure can effectively increase the deformation mode and expand the deformation range of the magnetic actuator, which is expected to make the magnetic actuator have a broad application prospect in the field of soft robots.

CRediT authorship contribution statement

Yinduan Gao: Conceptualization, Investigation, Writing – original draft. **Huaxia Deng:** Methodology, Funding acquisition, Writing – review & editing. **Haoming Pang:** Investigation. **Bing Liu:** Investigation, Formal analysis. **Zhenbang Xu:** Investigation. **Bochao Wang:** Investigation. **Xinglong Gong:** Supervision, Project administration, Resources, Funding acquisition, Writing – review & editing.

Declaration of Competing Interest

The authors declare that they have no known competing financial interests or personal relationships that could have appeared to influence the work reported in this paper.

Data availability

Data will be made available on request.

Acknowledgements

Financial supports from the National Natural Science Foundation of China (Grant Nos. 12132016, 12102424, 11972343), the Fundamental Research Funds for the Central Universities (WK2480000030, WK2480000009), the CAS Talent Introduction Program (KY2090000077), and the Anhui's Key R&D Program of China (202104a05020009) are gratefully acknowledged.

Appendix A. Supplementary material

Supplementary data to this article can be found online at https://doi.org/10.1016/j.compositesa.2023.107709.

References

[1] Barthelat F, Yin Z, Buehler MJ. Structure and mechanics of interfaces in biological materials. Nat Rev Mater 2016;1(4):16007.
[2] Li WB, Liu YJ, Leng JS. Light-actuated reversible shape memory effect of a polymer composite. Compos Part A-Appl S 2018;110:70–5.
[3] Paik JK, Hawkes E, Wood RJ. A novel low-profile shape memory alloy torsional actuator. Smart Mater Struct 2010;19(12):125014.
[4] Hong WY, Almomani A, Montazami R. Influence of ionic liquid concentration on the electromechanical performance of ionic electroactive polymer actuators. Org Electron 2014;15(11):2982–3297.
[5] Pu W, Wei FA, Yao LG, Xie SX. A review of humidity-driven actuator: toward high response speed and practical applications. J Mater Sci 2022;57(26):12202–35.
[6] Hajiesmaili E, Clarke DR. Dielectric elastomer actuators. J Appl Phys 2021;129 (15):151102.
[7] Peyer KE, Zhang L, Nelson BJ. Bio-inspired magnetic swimming microrobots for biomedical applications. Nanoscale 2013;5(4):1259–72.
[8] Qi J, Chen Z, Jiang P, Hu W, Wang Y, Zhao Z, et al. Recent progress in active mechanical metamaterials and construction principles. Adv Sci 2022;9(1): e2102662.
[9] Tawk C, Sariyildiz E, Alici G. Force control of a 3D printed soft gripper with built-in pneumatic touch sensing chambers. Soft Robot 2022;9(5):970–80.
[10] Kim Y, Zhao X. Magnetic soft materials and robots. Chem Rev 2022;122(5): 5317–64.
[11] Goh GD, Goh GL, Lyu Z, Ariffin MZ, Yeong WY, Lum GZ, et al. 3D printing of robotic soft grippers: toward smart actuation and sensing. Adv Mater Technol 2022;7(11):2101672.
[12] Zhu XC, Jing XJ, Cheng L. Magnetorheological fluid dampers: a review on structure design and analysis. J Intel Mat Syst Str 2012;23(8):839–73.
[13] Pang HM, Gao YD, Xuan SH, Gong XL. Effect of secondary particles on the microstructure and mechanical properties of magnetorheological plastomers. Compos Part A-Appl S 2022;153:106747–55.
[14] Stanier DC, Ciambella J, Rahatekar SS. Fabrication and characterisation of short fibre reinforced elastomer composites for bending and twisting magnetic actuation. Compos Part A-Appl S 2016;91:168–76.
[15] Zhang J, Wang Yu, Pang H, Sun S, Xu Z, Shen L, et al. Flexible anisotropic magneto-sensitive elastomer films with out-of-plane particle chain for bionic actuator. Compos Part A-Appl S 2021;150:106591.
[16] Fu Yu, Wei Z, Wan Z, Tian Ye, Zhao Z, Yang L, et al. Recent process of multimode stimuli-responsive flexible composites based on magnetic particles filled polymers: characteristics, mechanism and applications. Compos Part A-Appl S 2022;163: 107215.

[17] Diani J, Fayolle B, Gilormini P. A review on the Mullins effect. Eur Polym J 2009;45(3):601–12.
[18] Zhao RK, Kim Y, Chester SA, Sharma P, Zhao XH. Mechanics of hard-magnetic soft materials. J Mech Phys Solids 2019;124:244–63.
[19] Ding Li, Zhang J, Shu Q, Liu S, Xuan S, Gong X, et al. Magnetism-responsive anisotropic film with self-sensing and multifunctional shape manipulation. ACS Appl Mater Interfaces 2021;13(11):13724–34.
[20] Gong Di, Yang F, Lin D, Qian W, Li R, Li C, et al. Shape-programmable magneto-active elastomer composites for curve and biomimetic behavior imitation. Soft Matter 2021;17(47):10730–5.
[21] Zhao J, Li X, Tan Y, Liu X, Lu T, Shi M. Smart adhesives via magnetic actuation. Advanced Materials 2022;34(8):e2107748.
[22] Wang L, Zheng D, Harker P, Patel AB, Guo CF, Zhao X. Evolutionary design of magnetic soft continuum robots. Proc Natl Acad Sci U S A 2021;118(21):e2021922118.
[23] Li L, Xin C, Hu Y, Li R, Li C, Zhang Y, et al. On-demand maneuver of millirobots with reprogrammable motility by a hard-magnetic coating. ACS Appl Mater Interfaces 2022;14(46):52370–8.
[24] Kim Y, Parada GA, Liu S, Zhao X. Ferromagnetic soft continuum robots. Sci Robot 2019;4(33).
[25] Wu Z, Wang Qi, Huang J, Yue Y, Chen D, Shi Y, et al. The soft NdFeB/Ecoflex composites for soft robot with a considerable magnetostimulated shrinkability. Compos Sci Technol 2022;217:109129.
[26] Gao Y, Deng H, Zhang J, Shu Q, Xu Z, Cao X, et al. Magnetic actuator with programmable force distribution and self-sensing for bidirectional deformation control. Adv Mater Technol 2022;7(10):2200047.
[27] Gao W, Wang L, Wang X, Liu H. Magnetic driving flowerlike soft platform: Biomimetic fabrication and external regulation. ACS Appl Mater Interfaces 2016;8(22):14182–21419.
[28] Wu S, Ze Q, Zhang R, Hu N, Cheng Y, Yang F, et al. Symmetry-breaking actuation mechanism for soft robotics and active metamaterials. ACS Appl Mater Interfaces 2019;11(44):41649–58.
[29] Zhao W, Zhang F, Leng J, Liu Y. Personalized 4D printing of bioinspired tracheal scaffold concept based on magnetic stimulated shape memory composites. Compos Sci Technol 2019;184:107866.
[30] Cao XF, Xuan SH, Sun SS, Xu ZB, Li J, Gong XL. 3D printing magnetic actuators for biomimetic applications. ACS Appl Mater Interfaces 2021;13(25):30127–36.
[31] Jiang L, Wang Y, Wang X, Ning F, Wen S, Zhou Y, et al. Electrohydrodynamic printing of a dielectric elastomer actuator and its application in tunable lenses. Compos Part A-Appl S 2021;147:106461.
[32] Zolfagharian A, Gharaie S, Gregory J, Bodaghi M, Kaynak A, Nahavandi S. A bioinspired compliant 3D-printed soft gripper. Soft Robot 2022;9(4):680–769.
[33] Qi S, Guo H, Fu J, Xie Y, Zhu Mi, Yu M. 3D printed shape-programmable magneto-active soft matter for biomimetic applications. Compos Sci Technol 2020;188:107973.
[34] Kim Y, Yuk H, Zhao RK, Chester SA, Zhao XH. Printing ferromagnetic domains for untethered fast-transforming soft materials. Nature 2018;558(7709):274–329.
[35] Zhang Y, Wang Q, Yi S, Lin Zi, Wang C, Chen Z, et al. 4D printing of magnetoactive soft materials for on-demand magnetic actuation transformation. ACS Appl Mater Interfaces 2021;13(3):4174–84.
[36] Goyanes A, Allahham N, Trenfield SJ, Stoyanov E, Gaisford S, Basit AW. Direct powder extrusion 3D printing: fabrication of drug products using a novel single-step process. Int J Pharmaceut 2019;567:118471.
[37] Cao XF, Xuan SH, Gao YD, Lou CC, Deng HX, Gong XL. 3D printing ultraflexible magnetic actuators via screw extrusion method. Adv Sci 2022;9(16):2200898.